

DOUBLE-COUPLE EARTHQUAKE SOURCE: SYMMETRY AND ROTATION

Yan Y. Kagan

Department of Earth and Space Sciences, University of California,

Los Angeles, California 90095-1567, USA;

Emails: ykagan@ucla.edu, kagan@moho.ess.ucla.edu

Abstract. We consider statistical analysis of double couple (*DC*) earthquake focal mechanism orientation. The symmetry of *DC* changes with its geometrical properties, and the number of 3-D rotations one *DC* source can be transformed into another depends on its symmetry. Four rotations exist in a general case of *DC* with the nodal-plane ambiguity, two transformations if the fault plane is known, and one rotation if the sides of the fault plane are known. The symmetry of rotated objects is extensively analyzed in statistical material texture studies, and we apply their results to analyzing *DC* orientation. We consider theoretical probability distributions which can be used to approximate observational patterns of focal mechanisms. Uniform random rotation distributions for various *DC* sources are discussed, as well as two non-uniform distributions: the rotational Cauchy and von Mises-Fisher. We discuss how parameters of these rotations can be estimated by a statistical analysis of earthquake source properties in global seismicity. We also show how earthquake focal mechanism orientations can be displayed on the Rodrigues vector space.

Short running title: DOUBLE-COUPLE: SYMMETRY AND ROTATION

Key words: Earthquake focal mechanism, double couple, quaternion, material texture analysis, statistical analysis

1 Introduction

This paper addresses two problems: the random rotation of double-couple (*DC*) earthquake sources and how symmetry properties of these sources influence their rotation angle distribution and their display. Properties of earthquake focal mechanisms and methods for their determination are considered by Snoke (2003) and Gasperini & Vannucci (2003). Ekström *et al.* (2005, and references therein) discuss their extensive work on evaluating seismic moment tensors for global earthquakes.

In this paper we considered only the double-couple earthquake focal mechanism. For tectonic events non-double-couple mechanisms like the CLVD are likely due to various systematic and random errors in determining the mechanism (Frohlich & Davis 1999; Kagan 2003, 2009). These results suggest that routinely determined CLVD values would not reliably show the deviation of earthquake focal mechanisms from a standard *DC* model.

Snoke (2003) and Gasperini & Vannucci (2003) consider several equivalent representations for double-couple sources and their properties, and provide mathematical expressions for their mutual transformation. Krieger and Heimann (2012, and references therein) review routines for plotting moment tensors and focal mechanisms.

Two general techniques can be employed to study the 3-D rotation: orthonormal rotation matrices and normalized (unit) quaternions. The quaternion method has been used to evaluate these rotations in many investigations of earthquake focal mechanisms (see, for example, Kagan 1991; Frohlich & Davis 1999; Kagan 2009; Kagan & Jackson 2011). Kagan (2007) explains how ‘ordinary’ matrices and vectors can be used to obtain 3-D rotation parameters. Below we comment on the advantages and drawbacks of both methods.

Altmann’s (1986) book was a first monograph specifically dedicated to 3-D rotations [group $SO(3)$] and quaternions. At present quaternions are widely used to describe rota-

tions in space satellite and airplane dynamics (Kuipers 1999) and simulations of virtual reality, robotics and automation (Hanson 2006; Dunn & Parberry 2011). These last three monographs explain quaternions in a more accessible manner. Many journal articles (see references in these monographs and in Kagan 2009) discuss practical application of quaternions for analyzing the 3-D rotations.

However, the above publications do not consider the symmetry properties of rotated objects or how symmetry influences orientation analysis. As Kagan (1990; 1991; 2007; 2009) indicated, the techniques considered in those publications cannot be used for the *DC* source orientation studies without major modifications, because of the *DC* symmetry properties, described in Section 2. The only scientific discipline where symmetry is extensively considered in 3-D rotation analysis is study of material texture (Handscomb 1958; Mackenzie 1958; Grimmer 1979; Frank 1988; Heinz & Neumann 1991; Morawiec, 2004; Meister & Schaeben 2005; Schaeben 2010). In this paper (Section 3) we discuss applying these results to *DC* source investigations. In Section 4 we consider theoretical probability distributions used to approximate observational patterns of focal mechanisms. Section 5 is dedicated to the statistical analysis of earthquake source properties in global seismicity. Using the results of Section 3 we also show how earthquake focal mechanism orientations can be displayed in the Rodrigues vector space. Section 6 and Section 7 summarize our results.

2 Focal mechanism symmetry

Depending on the known properties of double-couple earthquake focal mechanism, we consider three types of earthquake source symmetry (Kagan 1990):

- 1. *DC1* – double couple with no symmetry or the identity (*I*) symmetry, if the focal plane and its sides are known;

- 2. *DC2* – double couple with C_2 , order 2 cyclic symmetry, i.e., the focal plane is known, but its sides are not;
- 3. *DC4* – double couple with nodal-planes that not distinguishable; it has D_2 , order 2 dihedral symmetry.

These earthquake source symmetries correspond to the following crystallographic symmetries considered in material texture analysis (see, for instance, Morawiec 2004). *DC4* has an orthorhombic symmetry (as in a rectangular right parallelepiped or a rectangular box with unequal sides); *DC2* has a monocline symmetry (as in a 3-D prism with two angles of 90° and one arbitrary angle); *DC1* has a triclinic, or no symmetry.

Fig. 1 displays the geometry of the *DC* source (Aki & Richards 2002). It represents the quadrupolar ‘beachball’ radiation patterns of earthquakes. The focal plots involve painting on a sphere the sense of the first motion of the primary P-waves: solid for compressional motion and open for dilatational. The two orthogonal nodal planes separating these areas are the fault and the auxiliary planes. During routine determination of focal mechanisms, it is impossible to distinguish between these planes, a property called ‘nodal-plane ambiguity.’ The planes’ intersection is the null-axis (called **b**-axis), the **p**-axis is in the middle of the open lune, and the **t**-axis is in the middle of the closed lune. These three axes are called the ‘principal axes of an earthquake focal mechanism,’ and their orientation defines the mechanism.

To make the focal mechanism picture unique, the eigenvectors are pointed down in regular representations. However, the handedness of the coordinate system formed by the vectors can change as the result of such an assignment. The systems of the opposing handedness cannot be rotated one into another. In most of our considerations, we use the right-handed coordinate system placed at each earthquake centroid.

Fig. 2 displays four examples of the right-handed coordinate system for a *DC4* source.

The system can be arbitrarily rotated, and the handedness of the system is preserved. The left-handed system can be obtained in this picture if one inverts the direction of any individual axis or of all three axes. If the direction of two axes is reversed, the handedness of the system is preserved.

The earthquake focal plane can often be determined by inverting the higher-rank point seismic moment tensors (McGuire *et al.* 2001; Chen *et al.* 2010) or by the aftershock pattern. The face/side (up/down or foot/hanging wall) of a focal plane generally is unknown. In such a case the *DC* focal mechanism has a C_2 symmetry; we call it *DC2*.

Finally, the face or the side of the focal plane can be known; it is shown in Fig. 1 by symbols *A* and *B*. Such a source is called *DC1*. Fig. 3 illustrates the difference between *DC2* and *DC1* mechanisms. If a cylinder of one material is rotated in a half-space of another material, the two *DC1* sources ‘1’ and ‘2’ would have a rotation angle of 180° . If they are considered as *DC2* sources, two angles 0° and 180° are possible to rotate one mechanism into another.

In Fig. 2, any of the configurations appropriately rotated can represent a *DC1* source, but only pairs (a)-(b) or (c)-(d) correspond to a *DC2* mechanism. All four diagrams correspond to a *DC4* source.

3 Earthquake focal mechanism and material texture statistics

Frank (1988) proposes using the Rodrigues vector space to represent 3-D rotation of symmetrical objects. This representation has an advantage: under any transformation of the Rodrigues map corresponding to a change of the reference orientation, straight lines transform into straight lines, and planes into planes.

For an object with the non-identity symmetry, accepted points lie in a region around the origin, which is called ‘the fundamental zone of the map.’ It is a polyhedron, bounded by the planes which are orientationally equidistant between the origin and the neighboring equivalent point by a symmetry rotation to the origin. Any points lying outside one of these planes have an equivalent point lying inside the fundamental zone (Frank 1988). For an orthorhombic crystal with three orthogonal axes, the fundamental zone is a cube, with its six faces orthogonal to the axes at a distance from the origin of $\tan \pi/4 = 1$ (Frank 1988). The cube is surrounded by three neighboring zones, each divided into two at infinity.

Fig. 4 shows the fundamental zone for a $DC4$ source (Heinz & Neumann, 1991, Fig. 7). It is a cube with corner coordinates $x_1 = \pm 1.0$; $x_2 = \pm 1.0$; $x_3 = \pm 1.0$. Owing to the $DC4$ symmetry, an octant of the cube contains full information about the orientation distribution for uniformly random rotation. This octant is called the ‘MacKenzie cell’ (Morawiec & Field 1996, see also their Fig. 1 displaying the cells for the D_3 and D_4 symmetries).

Each point *inside* the cube uniquely corresponds to a certain orientation/rotation with a minimum rotation angle $\Phi_{\min} \leq 120^\circ$. The points in the inscribed sphere of the cube correspond to the rotations with angles $\Phi_{\min} \leq 90^\circ$. The other three rotation angles are situated outside the fundamental zone. For example, the point of the zero rotation is located at the cube center, whereas three other rotation points are at infinity: $x_1 = \pm\infty$; $x_2 = \pm\infty$; $x_3 = \pm\infty$, corresponding to 180° rotations. These points at $\pm\infty$ are equivalent (Altmann 1986). Similarly, for any point inside the cube, three points outside correspond to the rotations with angles $\Phi > \Phi_{\min}$.

However, when a point moving orthogonally from the origin reaches a cube face, it simultaneously appears on the opposite face: two 90° rotations produce the same effect (Fig. 5). This means that when we determine the minimum angle Φ_{\min} for cyan point rotations shown in Fig. 5 using the program developed by Kagan (1991), we find two equal

solutions. The remaining two angles are greater than Φ_{\min} (see also the next Section).

If a point on one face moves to an edge, the ‘identical’ point on the opposite face simultaneously moves to another edge until both points reach the middle of the edges. This orientation corresponds to the rotation $\Phi \approx 109.5^\circ$, and Fig. 6 shows that there are three equivalent points at the edges. The third point appears as it moves from the outside of the cube to the third edge. As in Fig. 5, this means that three equal angles Φ_{\min} would be obtained. Finally, when a point is at a vertex, as shown in Fig. 7, three other vertices correspond to the same rotation $\Phi = 120^\circ$ (Frank 1988), i.e., all four rotation angles are Φ_{\min} .

This arrangement of the orientations for the rotation angles $\Phi \geq 90^\circ$ describes a complex topology for *DC4* source rotation. This topology involves projective or Möbius transformation (Altmann 1986; Frank 1988). Full analysis of the *DC4* source orientation, when and if performed, would involve very intricate investigations of rotation angle transformations due to source symmetry.

The Rodrigues space has no special advantages in displaying the orientation distribution for two other sources: *DC2* and *DC1*. For *DC2* the fundamental zone overlaps the entire Rodrigues space. For C_2 symmetry the fundamental zone is bounded by two planes perpendicular to the **b**-axis, each at the distance $\tan(\pi/4) = 1$ from 0. For a *DC1* source, the whole Rodrigues space up to infinity is included. In these cases other spaces are more convenient in displaying the 3-D rotation distribution (Frank 1988; Morawiec & Field, 1996). Altmann (1986, pp. 164-176) explains the projective or Möbius topology of rotations in the quaternion parametric ball for non-symmetrical objects.

4 Rotation of double couple earthquake sources

4.1 *DC* symmetry and rotation angle

In our earlier paper (Kagan 1991) we considered the inverse problem of the *DC4* source rotation, i.e., given two earthquake focal mechanisms to determine all the 3-D rotations by which one mechanism can be rotated into another. As we showed, the *DC4* symmetry results in four such rotations with angle Φ range $0^\circ \leq \Phi < 180^\circ$ (cf. Fig. 2). For most practical purposes, the rotation with a minimum angle Φ_{\min} can be selected. Following the material texture designation (Morawiec 2004, p. 115), we sometimes refer to general rotation angles as ‘misorientation angles’ and the minimum rotation angle as the ‘disorientation angle.’

Here we consider how to compute the rotation of a *DC1* source needed to align it with some reference *DC1* source. It is unlikely that sufficient data would exist on *DC1* sources for a statistical study of their distribution. However, in some cases we need to measure their angle of disorientation or the angular distance. Moreover, if the disorientation angle between two *DC1* sources is large, it would be almost impossible to identify their fault planes and plane faces. Small rotation angles for such focal mechanisms are likely to correspond to Φ_{\min} for the *DC4* source, as mentioned above.

To compute the disorientation of a *DC1* source, we can modify our FORTRAN program listed in Kagan (1991). When a fault plane and its face are known, a focal mechanism would be better specified through a fault plane geometry (Aki & Richards 2002, Figs. 4.13 and 4.20) with three angles: strike or azimuth (ϕ), dip (δ), and rake (λ). Usually the range of these angles is taken as follows: $0^\circ \leq \phi < 360^\circ$, $0^\circ \leq \delta < 90^\circ$, $-180^\circ \leq \lambda < 180^\circ$. The problem arises when comparing two sources if the dip (δ) of one focal plane exceeds 90° , so that a foot wall of one mechanism becomes a hanging wall for another source (Aki & Richards 2002). To simplify the calculations in our program (see below), we extend the δ

range to 180° .

If the face/side of a fault plane is unknown, as shown in Fig. 3, we need to calculate the second angle of the rotation for the *DC2* source. As with the *DC1* source, the data on *DC2* sources are sparse and insufficient for a statistical study, but we need a technique to measure their angles of disorientation. An easy way to accomplish this measurement would be to change the strike of the fault plane by 180° and change the rake sign. The modified `DC1ROT.FOR` program is available at <http://jumpy.igpp.ucla.edu/~kagan/dc1rot.for>.

In this program we use the quaternion technique to determine the rotation angle and the rotation axis parameters to transform one *DC* source into another. Quaternions are used because for rotation angle Φ close or equal to 180° , the matrix method cannot determine the rotation axis parameters (Kagan, 2007).

Kagan (2009, Appendices *A* and *B*) discusses normalized quaternions and their relation to the *DC4* source. Representations for the *DC4* by seismic moment tensors as well as by orthonormal matrices are considered. A quaternion representation allows a relatively easy determination of the rotation angle and the axis parameters for the *DC4* earthquake focal mechanism (Kagan 1991).

If only the rotation angle is needed, then one can use a scalar (dot) product of two quaternions (Hanson 2006, p. 65; Dunn & Parberry 2011, p. 255) to determine the angle:

$$\cos(\Phi/2) = \mathbf{q}^a \cdot \mathbf{q}^b = q_1^a q_1^b + q_2^a q_2^b + q_3^a q_3^b + q_4^a q_4^b, \quad (1)$$

where \mathbf{q}^i are normalized quaternions for each *DC* source and q_j are the quaternion's components.

In our program we first compute the orthonormal matrix for each *DC* source and then determine the corresponding normalized quaternion. There is a possibility of losing precision when converting a matrix to a quaternion (Shepperd 1978; Horn 1987). A certain computa-

tion technique should be applied to avoid this. We used a similar technique in our programs DCROT.FOR (Kagan 1991, the end of the SUBROUTINE QUATFPS) and in DC1ROT.FOR (see above).

4.2 Rotation angle distribution

4.2.1 Uniform random rotation of *DC* sources

The distribution of the uniform random rotation for *DC* sources constitutes a reference for distributions occurring in earthquake focal mechanisms where we expect the distributions to be partially random. These stochastic distributions can be analytically calculated by taking into account the sources' symmetry.

A distribution of the minimum angle Φ_{\min} for a uniform random rotation of the *DC4* source was obtained by Kagan (1990, Eqs. 3.1-3.3), using the results by Handscomb (1958) and Mackenzie (1958) for the random disorientation of two cubes. The probability density function (PDF) is

$$f(\Phi) = (4/\pi)(1 - \cos \Phi) \quad \text{for } 0 \leq \Phi \leq \pi/2; \quad (2)$$

$$f(\Phi) = (4/\pi)(3 \sin \Phi + 2 \cos \Phi - 2) \quad \text{for } \pi/2 \leq \Phi \leq \Phi_S; \quad (3)$$

and

$$f(\Phi) = \left. \begin{aligned} & (4/\pi) \left\{ 3 \sin \Phi + 2 \cos \Phi - 2 - \right. \\ & (6/\pi) \left[2 \sin \Phi \arccos \left(\frac{1+\cos \Phi}{-2 \cos \Phi} \right)^{1/2} - \right. \\ & \left. \left. (1 - \cos \Phi) \arccos \frac{1+\cos \Phi}{-2 \cos \Phi} \right] \right\} \\ & \text{for } \Phi_S \leq \Phi \leq \frac{2\pi}{3}, \end{aligned} \right\} \quad (4)$$

where

$$\Phi_S = 2 \arccos(3^{-1/2}) = \arccos \left(-\frac{1}{3} \right) \approx 109.47^\circ. \quad (5)$$

For the *DC2* source a similar PDF is

$$f(\Phi) = (2/\pi)[1 - \cos(\Phi)] \quad \text{for } 0 \leq \Phi \leq \pi/2; \quad (6)$$

and

$$f(\Phi) = (2/\pi) \sin(\Phi) \quad \text{for } \pi/2 \leq \Phi \leq \pi. \quad (7)$$

For the *DC1* source the function is

$$f(\Phi) = (1/\pi)[1 - \cos(\Phi)] \quad \text{for } 0 \leq \Phi \leq \pi. \quad (8)$$

Grimmer (1979), also following Handscomb (1958) and Mackenzie (1958) results, obtained similar analytic expressions for a completely random rotation of orthorhombic, monoclinic, and triclinic crystals (equivalent in symmetry to the *DC* earthquake source with various restrictions described above). He listed median angles as well as their mean and standard deviations for all these distributions. Morawiec (1995; 2004, pp. 117-119) derived these distributions by integration in the Rodrigues space.

4.2.2 Non-uniform distributions of random rotations

Two non-uniform rotation angle distributions are useful in analyzing earthquake focal mechanism rotation: the rotational Cauchy law (Kagan 1982, 1992) and von Mises-Fisher/Bingham rotational distribution (Kagan 1992, 2000; Schaeben 1996; Mardia & Jupp 2000, pp. 289-292; Morawiec 2004, pp. 88-89).

The Cauchy distribution is especially important for representing earthquake geometry, since it can be shown by theoretical arguments (Zolotarev 1986, pp. 45-46; Kagan, 1990) and simulations (Kagan 1990) that the stress tensor in a medium with random defects follows this distribution. The Cauchy law is a *stable* distribution (Zolotarev, 1986). The stable distributions are essential for two reasons: a) They are invariant under addition of random

variables; b) Stable distributions have a power-law tail, i.e., they are asymptotically scale-invariant.

The probability density function (PDF) of the rotational Cauchy distribution can be written as (Kagan 1982; 1990)

$$f(\Phi) = \frac{2}{\pi} \left[\frac{\kappa A^2 (1 + A^2)}{(\kappa^2 + A^2)^2} \right] = \frac{4 \kappa [1 - \cos(\Phi)]}{\pi [1 + \kappa^2 + (\kappa^2 - 1) \cos(\Phi)]^2}, \quad \text{for } 180^\circ \geq \Phi \geq 0^\circ, \quad (9)$$

where $A = \tan(\Phi/2)$. The scale parameter κ of the Cauchy distribution represents the degree of *incoherence* or *complexity* in a set of earthquake focal mechanisms. The cumulative rotational Cauchy distribution can be written as

$$F(\Phi) = \frac{2}{\pi} \left[\arctan(A/\kappa) - \frac{A \times \kappa}{A^2 + \kappa^2} \right]. \quad (10)$$

The Cauchy distribution is assumed to be axisymmetric on the quaternion hypersphere S^3 . This means that the rotation axis poles are distributed uniformly over a regular S^2 sphere. For a general case, the axes distribution for earthquake focal mechanisms may need to be specified as non-uniform. In that case certain rotations would be preferred depending on the focal mechanism of a reference event. However, we have not yet advanced to this stage (see Section 5).

The von Mises-Fisher/Bingham distribution for the 3-D orientation is widely discussed in literature (Schaeben 1996; Mardia & Jupp 2000; Morawiec 2004). Schaeben (1996) and Morawiec (2004) show that this distribution is essentially equivalent to the Bingham distribution. The von Mises-Fisher distribution is a Gaussian-shaped function concentrated near the zero angle. This distribution can be implemented to model random errors in determining focal mechanisms. The distribution has many forms. However, even the simplest axially symmetric expressions, due to the complexity of normalization, represent difficult computation.

For small values of the standard error σ_Φ , the von Mises-Fisher-type distribution is equivalent to the rotational Maxwell law used by Kagan & Knopoff (1985) and Kagan (1992). The latter distribution is obtained by generating a 3-D normally distributed random variable \mathbf{u} (u_1, u_2, u_3) with the standard deviation $\sigma_{\mathbf{u}}$ ($\sigma_{u_1}, \sigma_{u_2}, \sigma_{u_3}$) and then calculating the unit quaternion

$$\begin{aligned} q_0 &= 1/\sqrt{1 + u_1^2 + u_2^2 + u_3^2}, \\ q_i &= u_i/\sqrt{1 + u_1^2 + u_2^2 + u_3^2}, \quad \text{for } i = 1, 2, 3. \end{aligned} \quad (11)$$

The 3-D rotation angle is calculated

$$\begin{aligned} \Phi &= 2 \arccos(q_0) \approx 2 \arccos\left(1 - (u_1^2 + u_2^2 + u_3^2)/2\right) \\ &\approx 2 \arcsin \sqrt{u_1^2 + u_2^2 + u_3^2} \approx 2\sqrt{u_1^2 + u_2^2 + u_3^2}. \end{aligned} \quad (12)$$

The final expression is twice the length of a vector in the 3-D space.

Since components of vector \mathbf{u} are normally distributed, the angle Φ (in degrees) follows the Maxwell distribution with

$$\sigma_\Phi = 360 \sigma_u / \pi, \quad (13)$$

where we assume that all components of $\sigma_{\mathbf{u}}$ are equal ($\sigma_{u_1} = \sigma_{u_2} = \sigma_{u_3} = \sigma_u$). For $180^\circ \geq \Phi \geq 0^\circ$ the Maxwell PDF is

$$\psi(\Phi) = \sqrt{\frac{2}{\pi}} \times \frac{\Phi^2}{\sigma_\Phi^3} \times \exp\left[-\Phi^2/(2\sigma_\Phi^2)\right]. \quad (14)$$

This equation describes the distribution of a vector length in three dimensions, if the vector components have a Gaussian distribution with a zero mean and a standard error σ_Φ . The Maxwell cumulative distribution function (CDF) is

$$\Psi(\Phi) = \operatorname{erf}\left(\frac{\Phi}{\sigma_\Phi \sqrt{2}}\right) - \sqrt{\frac{2}{\pi}} \times \frac{\Phi}{\sigma_\Phi} \times \exp\left[-\Phi^2/(2\sigma_\Phi^2)\right], \quad (15)$$

where $\text{erf}(\cdot)$ is an error function.

The major problem with these non-uniform random distributions is that they do not consider the symmetry of the rotated object. When rotation angles are small, the distribution is concentrated around the zero angle neighborhood. For the *DC4* source as shown in Fig. 4, almost all distribution density would be inside the fundamental zone. However, for more spread out angle distributions, we should account for cases where the rotation angle exceeds the maximum angles (see, for example, Eqs. 2-5). Then the distribution would be folded back into the fundamental zone.

Mason & Schuh (2009) propose to convolve angle distribution with appropriate 3-D spherical or 4-D hyperspherical harmonics to obtain a new angle distribution which fits into the fundamental zone. It is not clear whether such calculations can be made analytically. Simulation seems the only practical way to transform both Cauchy and von Mises/Fisher distributions for the D_2 symmetric case (i.e., for maximum Φ_{\min} rotation angle 120°). Kagan (1992, Fig. 3c) produced such distributions. Fig. 8 below plots the appropriate Cauchy distribution which is reduced to $\Phi_{\min} \leq 120^\circ$.

5 Focal mechanisms statistics

5.1 Disorientation angle statistics

Since there is no general model of earthquake focal mechanism distribution, we need to study the distribution of mechanisms in earthquake catalogs empirically to infer their properties. How various tectonic and geometrical factors shape the distribution of earthquake sources should be studied as well. Such investigations are difficult because we are dealing with a multidimensional stochastic point process: earthquake size, occurrence time, location, and

source parameters serve as potential inputs to the distributions.

In this paper we are mostly interested in the distributions of rotation between two earthquake focal mechanisms. Even if we fix earthquake time, space, and magnitude interval, the *DC* rotation distribution depends on at least three variables: the rotation angle and two spherical coordinates of a rotation axis pole. Displaying all three degrees of freedom in a distribution presents a difficult problem. Therefore, in our previous investigations we studied partial distributions. For example, Kagan (1992, Figs. 6-9; 2009, Figs. 9,10) obtained various distributions of the rotation angle Φ_{\min} between two focal mechanisms. Below we first update our most important results on the distribution of the rotation angle Φ_{\min} , and then analyze a three-dimensional distribution of rotation angle and the axes in the Rodrigues space.

We used the Global Centroid Moment Tensor catalog (Ekström *et al.* 2005), referred to subsequently as GCMT. This catalog employs relatively consistent methods and reports tensor focal mechanisms. The GCMT catalog started in 1977, and is complete only for earthquakes with magnitudes of about 5.8 and larger. The present catalog contains more than 36,000 earthquake entries from 1977/1/1 to 2011/12/31.

Fig. 8 displays cumulative distributions of the rotation angle Φ_{\min} for shallow earthquake pairs with the magnitude threshold $m_t = 5.0$ that are separated by a distance of less than 50 km. We study whether the rotation of focal mechanisms depends on where the second earthquake of a pair is situated with regard to the first event. Thus, we measure the rotation angle for centroids located in 30° cones around each principal axis of the first event (see curves, marked the **t**-, **p**-, and **b**-axes).

The curves in Fig. 8 are narrowly clustered, with about 95% of angles less than 90° , within an inscribed sphere of the fundamental zone (Fig. 4). This pattern can be compared to the uniform rotation (Eqs. 2-4) for which 72.7% ($2 - 4/\pi$) of angles are within 90° . The

curves are obviously well approximated by the *DC* rotational Cauchy distribution (Eq. 9). This distribution is characterized by a parameter κ ; a smaller κ -value corresponds to the rotation angle Φ_{\min} concentrated closer to zero. Thus, regardless of spatial orientation, all earthquakes have focal mechanisms similar to a nearby event. Earthquakes in the cone around the **b**-axis correspond to a smaller κ -value than events near the other axes. These results are similar to those shown in Fig. 6 by Kagan (1992) or Fig. 9 by Kagan (2009).

Fig. 9 and Fig. 10 show the disorientation angle distribution for the magnitude cutoff $m_t = 5.8$. As may be expected for the higher magnitude, the angles are concentrated closer to zero, and the difference between the curves corresponding to various cones increases. Maxwell distribution curves are shown to illustrate possible behavior of the angle distributions near zero. The $\sigma_\Phi = 7.5^\circ$ parameter of the distribution is small, compared to the distribution range ($120^\circ \geq \Phi \geq 0^\circ$). Therefore, the curves are concentrated close to zero; we do not need simulation to consider the curve behavior for large values of Φ_{\min} , as done, for example, in Fig. 3c by Kagan (1992).

The difference in the distribution curves corresponding to various focal mechanism axes suggests that the Cauchy distribution parameter κ depends upon the geometry of a fault system. Contrary to our assumptions (Eq. 9), poles of rotation axes are not uniformly distributed over the S^2 sphere.

5.2 Distributions of rotation axes

Mackenzie (1964) derived the distribution of the rotation axes for cubic symmetry. Morawiec (1996) obtained distributions of rotation axes for any symmetric object encountered in material texture analysis. Using his results we can write down the distribution of rotation axes for the D_2 symmetry: the *DC4* source. The Mackenzie cell is shown in Fig. 4. We designate the coordinate axes as x_i , $i = 1, 2, 3$, and the distribution depends on distance

from the origin. As seen in Fig. 4, the distribution should have a 3-fold cyclic symmetry C_3 around the origin or around the cube vertex. Then the PDF for the axes density is

$$p(\rho) = \frac{16}{\pi^2} \left[\arctan(\rho) - \rho/(1 + \rho^2) \right], \quad (16)$$

where the distance $\rho = \sqrt{x_1^2 + x_2^2 + x_3^2}$. For small value of ρ , $p(\rho) \propto \rho^3$.

Fig. 11 displays the $p(\rho)$ density. Its values at $\rho = 1$, $\rho = \sqrt{2}$, and $\rho = \sqrt{3}$ correspond to appropriate values for the D_2 symmetry (Morawiec 1996, Table 2). These ρ -values correspond to the rotation angles $\Phi = 90^\circ, 109.5^\circ$, and 120.0° , respectively. For $\Phi \leq 90^\circ$ the rotation axes are distributed uniformly over the S^2 sphere, but they intersect the sphere near the cube vertex close to $\Phi = 120^\circ$.

In Fig. 12 we show the distribution of the rotation poles for the second earthquake focal mechanism on a reference sphere of the first event. Because of the symmetry of the $DC4$ source, we reflect the point pattern on our reference sphere at the planes perpendicular to all axes. Thus, the distribution can be shown on a spherical octant. We use the Lambert azimuthal equal-area projection. The points concentrate near the projections of the far edges of the MacKenzie cell (see Fig. 4) and around the cube vertex which corresponds to the disorientation angle $\Phi = 120^\circ$.

5.3 Rodrigues space statistics and display

A major problem in the orientation visualizing is the high dimensionality of the 3-D rotation space: the orthogonal matrices are characterized by nine values, the seismic moment tensor requires five or six variables, and the normalized quaternion needs four values. The real number of degrees of freedom for a 3-D rotation is three. Thus, in principle, an orientation distribution can be shown in a 3-D diagram.

Frank (1988), Neumann (1992) and Morawiec & Field (1996) propose using the Rodrigues

vector space to display the disorientation of symmetric objects in a fundamental zone as a point in the space. The point coordinates are calculated as follows: the length of a vector ζ is

$$\zeta = \tan(\Phi/2). \quad (17)$$

where Φ_{\min} is the rotation angle. Three coordinates of a point in the zone are

$$\begin{aligned} x_1 &= \zeta \times \sin(\theta) \sin(\phi); \\ x_2 &= \zeta \times \sin(\theta) \cos(\phi); \\ x_3 &= \zeta \times \cos(\theta), \end{aligned} \quad (18)$$

where θ is the colatitude, and ϕ is the azimuth of the rotation axis. As shown in Fig. 4, we identify x_1 with the \mathbf{p} -axis; similarly $x_2 = \mathbf{t}$ and $x_3 = \mathbf{b}$.

We obtain a distribution diagram for a set of disorientations. One way to display such a diagram of the fundamental zone is through stereo-pairs (Neumann 1992). Morawiec & Field (1996) display the distribution of misorientation parameters by points in some parallel sections of the fundamental zone.

Fig. 13 shows a distribution for randomly rotated *DC4* sources in a central section of the fundamental zone of the Rodrigues space. Fig. 14 displays a similar distribution of the earthquake focal mechanism orientation in the GCMT catalog. As Figs. 8-10 demonstrate, the distribution of the rotation angles for earthquake sources is strongly concentrated close to 0° . If we compare Fig. 13 and Fig. 14, this concentration is marked in the fundamental zone display.

Table 1 summarizes earthquake focal mechanism disorientation patterns in the fundamental zone of *DC4*. The total number of events N with the magnitude above the threshold is shown, as well as the total number of pairs N_p with centroids separated by less than 50 km. N_c is the pair numbers in the central zone shown in Fig. 14. Although the central section

occupies only 5% of the zone, close to 50% of the pairs are there due to a tight concentration of rotation angles near the zero value. For simulated events in the central zone, the number N_c is about 7% of the total (see Fig. 13).

We also display the correlation coefficients of the point scatter field. Whereas for earthquake focal mechanisms the coefficients ρ_{bp} and ρ_{bt} are close to zero, the ρ_{pt} and ρ'_{pt} coefficients are non-zero, testifying to a certain pattern of focal mechanism rotation. Fig. 11 in Kagan (2009) also shows that rotation axes are concentrated closer to the \mathbf{t} -axis. All correlation coefficients for the simulated mechanisms are around zero. A more detailed statistical analysis of this pattern will be carried out in our future work.

The values of the average rotation angle and its standard deviation ($\bar{\Phi} \pm \sigma_{\Phi}$) show that for larger earthquakes both variables are smaller. This may be caused by a higher accuracy in determining focal mechanism for stronger shocks (Kagan 2003). For simulated focal mechanisms, the $\bar{\Phi} \pm \sigma_{\Phi}$ values are close to the theoretical estimates for orthorhombic symmetry (Grimmer 1979).

6 Discussion

Quantitative study of earthquake focal mechanisms is an important prerequisite for understanding earthquake rupture. Though these investigations began in the mid 1950s, publications have been mostly descriptive until now; relatively little modelling and rigorous statistical analysis have been performed. A major difficulty in analyzing focal mechanisms is both the high dimensionality and non-commutativity of the 3-D rotations. This presents a major challenge in analyzing a set of focal mechanisms.

Several papers (Kagan, 1992, 2000, 2009) have investigated statistical distributions of earthquake focal mechanisms. We found that the disorientation angle is close to zero for

spatially close earthquakes, and the angle decreases if the inter-earthquake time interval approaches zero. We also showed (Kagan, 2009) that the CLVD component of focal mechanism tensor is either zero or close to zero for most geometric barriers proposed as common features in an earthquake fault system.

However, the major challenges in describing and understanding the distributions of focal mechanisms still remain. As we see from Figs. 8-10, the angle distribution is not axially symmetric: in certain directions Φ_{\min} is larger than in others. Thus, the distributions used to approximate the angle pattern, like the rotational Cauchy distribution (Eqs. 9-10), need to be made more complex.

The distribution of rotation axes was not investigated as thoroughly as that for disorientation angles. There is still no theoretical model for approximating empirical data, but applying the Rodrigues space may render such analysis more manageable.

However, even these limited results contribute significantly to understanding of earthquake focal mechanism properties and allows certain quantitative applications for seismic risk evaluation. Kagan & Jackson (2011) explain that the forecasted tensor focal mechanism enables calculating an ensemble of seismograms for each point of interest on the Earth's surface. Moreover, the focal mechanism distribution allows us to estimate fault plane orientation for past earthquakes, through which we can identify a preferred rupture direction for future events.

The angle Φ_{\min} has also been used to directly compare moment tensors from two different earthquakes (Okal *et al.* 2011). It has as well been applied in comparing moment tensors computed for the same events through different techniques (Frohlich & Davis 1999; Pondrelli *et al.* 2007; Yang *et al.* 2012). Such comparisons can help refine the moment tensor algorithms and lower their computational cost, since they can reveal the relative importance of various assumptions implicit in the algorithms.

7 Conclusions

- 1. The symmetry properties of an earthquake double-couple focal mechanism are considered. Given available seismological and geologic information, three symmetries are possible: D_2 (dihedral symmetry), C_2 (cyclic symmetry), and I (identity). Determining the orientation or disorientation of the source depends on its symmetry.

- 2. Quaternion representation is the most convenient tool for analysing a double-couple 3-D rotation. A 3-D rotation requires at least three degrees of freedom for its characterization.

- 3. Several theoretical distributions to describe a 3-D rotation of double-couples are presented: random rotation, rotational Cauchy, and von Mises-Fisher.

- 4. The Rodrigues space, so extensively used in material texture analysis is applied to display and analyze earthquake focal mechanism distribution. This space allows us to represent 3-D patterns of how symmetric objects are oriented.

- 5. We illustrate the proposed methods by statistically analyzing the GCMT catalog of earthquake focal mechanisms.

Acknowledgments

I am grateful to Dave Jackson, Paul Davis, and Peter Bird of UCLA, as well as Maximilian Werner and Men Meier of ETH Zurich for useful discussion and suggestions. I thank Kathleen Jackson for editing and significant improvements in the text. The author appreciates partial support from the National Science Foundation through grants EAR-0944218, and EAR-1045876, as well as from the Southern California Earthquake Center (SCEC). SCEC is funded by NSF Cooperative Agreement EAR-0529922 and USGS Cooperative Agreement 07HQAG0008. Publication 0000, SCEC.

REFERENCES

- Aki, K. & Richards, P. 2002. *Quantitative Seismology*, 2nd ed., Sausalito, Calif., University Science Books, 700 pp.
- Altmann, S. L. 1986. *Rotations, Quaternions and Double Groups*, Clarendon Press, Oxford, pp. 317.
- Chen, P., T.H. Jordan, Li Zhao 2010. Resolving fault plane ambiguity for small earthquakes, *Geophys. J. Int.*, **181**(1), 493-501, DOI: 10.1111/j.1365-246X.2010.04515.x.
- Dunn, F. & I. Parberry 2011. *3D Math Primer for Graphics and Game Development*, A.K. Peters/CRC Press, 846 pp.
- Ekström, G., A. M. Dziewonski, N. N. Maternovskaya & M. Nettles 2005. Global seismicity of 2003: Centroid-moment-tensor solutions for 1087 earthquakes, *Phys. Earth planet. Inter.*, **148**(2-4), 327-351.
- Frank, F. C. 1988. Orientation mapping, *Metall. Trans. A*, **19**, 403-408.
- Frohlich, C. & S. D. Davis 1999. How well constrained are well-constrained T, B, and P axes in moment tensor catalogs?, *J. Geophys. Res.*, **104**, 4901-4910.
- Gasparini, P. & G. Vannucci 2003. FPSPACK: a package of FORTRAN subroutines to manage earthquake focal mechanism data, *Computers & Geosciences*, **29**(7), 893-901, DOI: 10.1016/S0098-3004(03)00096-7.
- Grimmer, H. 1979. Distribution of disorientation angles if all relative orientations of neighboring grains are equally probable, *Scripta Metallurgica*, **13**(2), 161-164, DOI: 10.1016/0036-9748(79)90058-9.
- Handscomb, D. C. 1958. On the random disorientation of two cubes, *Can. J. Math.*, **10**, 85-88.
- Hanson, A. J. 2006. *Visualizing Quaternions*, San Francisco, Calif., Elsevier, pp. 498.

- Heinz, A. & Neumann, P. 1991. Representation of orientation and disorientation data for cubic, hexagonal, tetragonal and orthorhombic crystals, *Acta Cryst. A*, **47**, 780-789.
- Horn, B. K. P. 1987. Closed-form solution of absolute orientation using unit quaternions, *J. Opt. Soc. Am. A*, **4**(4), 629-642.
- Kagan, Y. Y. 1982. Stochastic model of earthquake fault geometry, *Geophys. J. Roy. astr. Soc.*, **71**(3), 659-691.
- Kagan, Y. Y. 1990. Random stress and earthquake statistics: Spatial dependence, *Geophys. J. Int.*, **102**(3), 573-583.
- Kagan, Y. Y. 1991. 3-D rotation of double-couple earthquake sources, *Geophys. J. Int.*, **106**(3), 709-716.
- Kagan, Y. Y. 1992. Correlations of earthquake focal mechanisms, *Geophys. J. Int.*, **110**(2), 305-320.
- Kagan, Y. Y. 2000. Temporal correlations of earthquake focal mechanisms, *Geophys. J. Int.*, **143**(3), 881-897.
- Kagan, Y. Y., 2003. Accuracy of modern global earthquake catalogs, *Phys. Earth Planet. Inter.*, **135**(2-3), 173-209, doi:10.1016/S0031-9201(02)00214-5.
- Kagan, Y. Y. 2007. Simplified algorithms for calculating double-couple rotation, *Geophys. J. Int.*, **171**(1), 411-418, doi: 10.1111/j.1365-246X.2007.03538.x.
- Kagan, Y. Y. 2009. On the geometric complexity of earthquake focal zone and fault systems: A statistical study, *Phys. Earth Planet. Inter.*, **173**(3-4), 254-268, doi: 10.1016/j.pepi.2009.01.006.
- Kagan, Y. Y. & Jackson, D. D. 2011. Global earthquake forecasts, *Geophys. J. Int.*, **184**(2), 759-776, doi: 10.1111/j.1365-246X.2010.04857.x
- Krieger, L. & S. Heimann 2012. MoPaD – Moment tensor plotting and decomposition: A

- tool for graphical and numerical analysis of seismic moment tensors, *Seismol. Res. Lett.*, **83**(3), 589-595, doi:10.1785/gssrl.83.3.589.
- Kuipers, J. B. 1999. *Quaternions and Rotation Sequences: A Primer with Applications to Orbits, Aerospace and Virtual Reality*, Princeton, Princeton Univ. Press., 400 pp.
- Mackenzie, J. K. 1958. Second paper on statistics associated with the random disorientation of cubes, *Biometrika*, **45**, 229-240.
- Mackenzie, J.K. 1964. Distribution of rotation axes in random aggregate of cubic crystals, *Acta Metallurgica*, **12**(2), 223-225, DOI: 10.1016/0001-6160(64)90191-9.
- Mardia, K. V. & P. E. Jupp 2000. *Directional Statistics*, Chichester, New York, Wiley, 429 pp.
- Mason, J.K. & C.A. Schuh 2009. The generalized Mackenzie distribution: Disorientation angle distributions for arbitrary textures, *Acta Materialia*, **57**, 4186-4197.
- McGuire, J. J., Li Zhao & Jordan, T. H. 2001. Teleseismic inversion for the second-degree moments of earthquake space-time distributions, *Geophys. J. Int.*, **145**, 661-678.
- Meister, L. & H. Schaeben 2005. A concise quaternion geometry of rotations, *Math. Meth. Appl. Sci.*, **28**, 101-126.
- Moakher, M. 2002. Means and averaging in the group of rotations, *SIAM J. Matrix Anal. Appl.*, **24**(1), 1-16.
- Morawiec, A. 1995. Misorientation-angle distribution of randomly oriented symmetrical objects, *J. Applied Crystallography*, **28**(3), 289-293, DOI: 10.1107/S0021889894011088.
- Morawiec, A., 1996. Distributions of rotation axes for randomly oriented symmetric objects, *J. Applied Crystallography*, **29**(2), 164-169, DOI: 10.1107/S0021889895013641.
- Morawiec, A. 2004. *Orientations and Rotations: Computations in Crystallographic Textures*, Springer/Berlin, New York, pp. 200.

- Morawiec, A. & Field, D. P. 1996. Rodrigues parameterization for orientation and misorientation distributions, *Philos. Mag. A*, **73**(4), 1113-1130.
- Neumann, P., 1992. The role of geodesic and stereographic projections for the visualization of directions, rotations, and textures, *Phys. Stat. Sol. (a)*, **131**, 555-567.
- Okal, E. A., Borrero, J. C., & Chagui-Goff, C. 2011. Tsunamigenic predecessors to the 2009 Samoa earthquake, *Earth-Sci. Rev.*, **107**, 128-140.
- Pondrelli S., Salimbeni, S., Morelli, A., Ekström, G., Boschi, E. 2007. European-Mediterranean regional centroid moment tensor catalog: Solutions for years 2003 and 2004, *Phys. Earth Planet. Inter.*, **164**(1-2), 90-112.
- Schaeben, H. 1996. Texture approximation or texture modelling with components represented by the von Mises-Fisher matrix distribution on $SO(3)$ and the Bingham distribution on S_+^4 , *J. Appl. Cryst.*, **29**, 516-525.
- Schaeben, H. 2010. Special issue on spherical mathematics and statistics, *Math Geosci.*, **42**, 727-730, DOI 10.1007/s11004-010-9304-7.
- Shepperd, S. W. 1978. Quaternion from rotation matrix, *J. Guidance and Control*, **1**, 223-224.
- Snoke, J. A. 2003. FOCMEC: FOcal MEChanism determinations, *International Handbook of Earthquake and Engineering Seismology* (W. H. K. Lee, H. Kanamori, P. C. Jennings & C. Kisslinger, Eds.), Academic Press, San Diego, Chapter 85.12. pp. 1629-1630.
- Yang, W., E. Hauksson, & P. M. Shearer 2012. Computing a large refined catalog of focal mechanisms for southern California (1981-2010): Temporal stability of the style of faulting, *Bull. Seismol. Soc. Amer.*, **102**, 1179-1194, doi:10.1785/0120110311.
- Zolotarev, V. M. 1986. *One-Dimensional Stable Distributions*, Amer. Math. Soc., Providence, R.I., pp. 284; Russian original 1983.

Table 1: Properties of disorientation point scatter in the fundamental zone of a *DC4* source

#	m_t	N	N_p	N_c	ρ_{pt}	ρ_{bp}	ρ_{bt}	ρ'_{pt}	$\bar{\Phi} \pm \sigma_{\Phi}$
1	5.6	9,615	43,611	18,381	0.126	0.026	0.013	0.170	31.6 ± 27.5
2	5.8	6,160	19,367	8,725	0.117	0.022	-0.001	0.127	29.9 ± 26.9
3	6.25	2,154	2,741	1,244	0.274	-0.016	-0.026	0.257	28.5 ± 26.1
4	Simul.	25,000	25,000	1,754	-0.012	-0.002	0.002	-0.015	75.0 ± 21.0

Notes: The GCMT catalog time interval is 1977/1/1–2011/12/31. N is the total number of events with magnitude $m \geq m_t$; N_p is the total number of event pairs; N_c is the number of event pairs in the central section; ρ_{pt} , ρ_{bp} , and ρ_{bt} are the correlation coefficients for all points; ρ'_{pt} is the correlation coefficient for all points within the central section; $\bar{\Phi} \pm \sigma_{\Phi}$ is the average disorientation angle and its standard deviation.

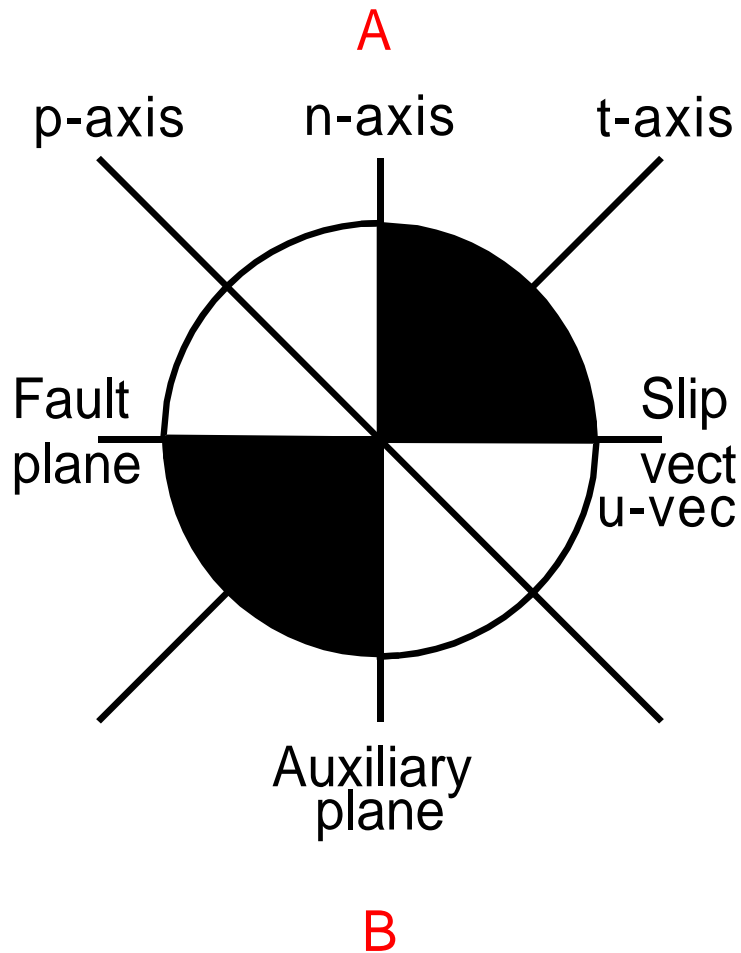


Figure 1:

Schematic (beachball) diagram of the *DC* earthquake focal mechanism and its quadrupole radiation patterns. The null (**b**) axis is orthogonal to the **t**- and **p**-axes, or it is located on the intersection of fault and auxiliary planes, i.e., perpendicular to the paper sheet in this display. The **n**-axis is normal to the fault-plane; **u** is a slip vector.

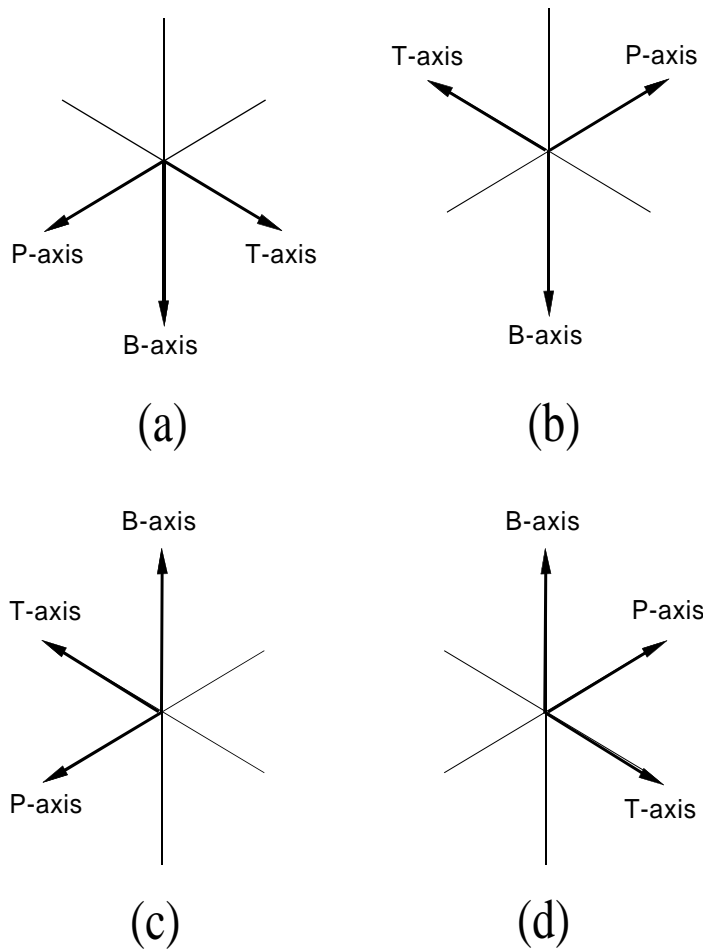


Figure 2:

Four schematic diagrams of earthquake focal mechanism, having the $DC4$ symmetry. The right-hand coordinate system is used.

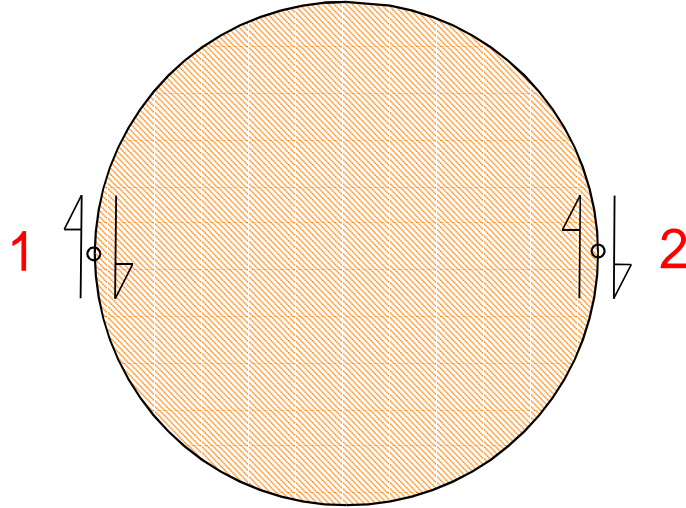


Figure 3: Schematic diagram of earthquake focal mechanism *DC2*.

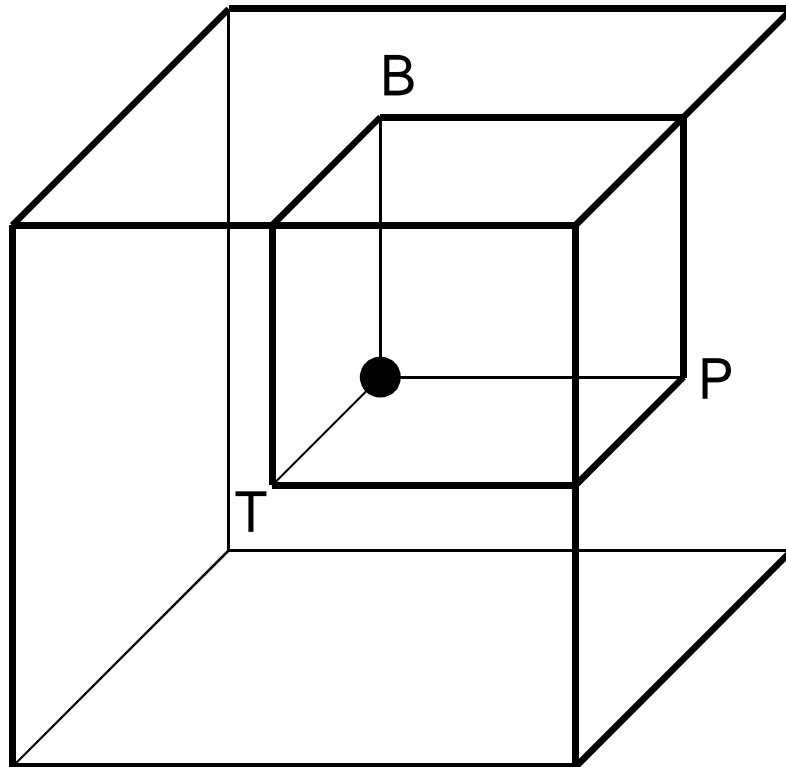


Figure 4:

Fundamental zone display for $DC4$ source. The \mathbf{b} , \mathbf{p} , and \mathbf{t} -axes of the source are shown.

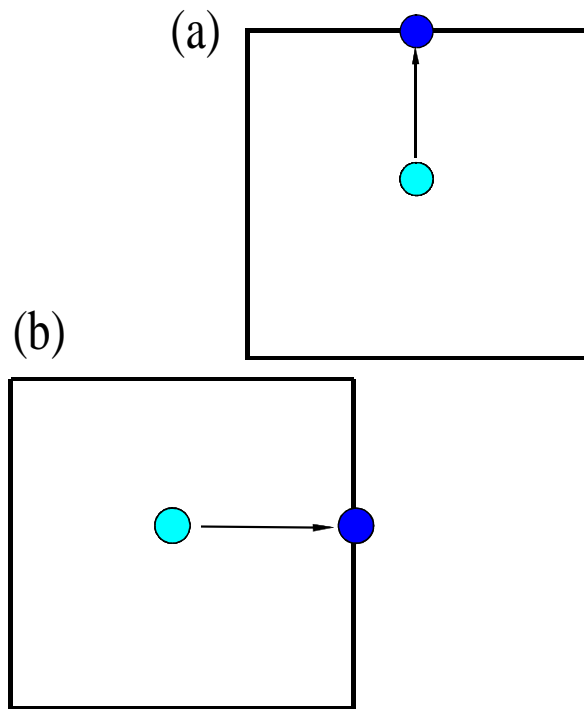


Figure 5:

Fundamental zone display for $DC4$ source. Colors show two face points corresponding to one source orientation with the angle $\Phi \geq 90^\circ$.

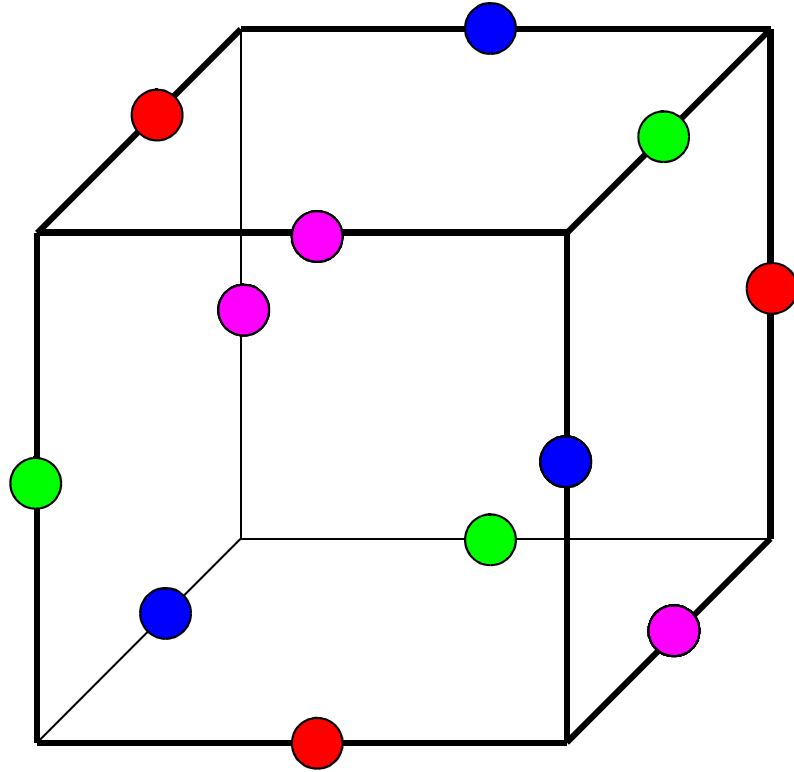


Figure 6:

Fundamental zone display for $DC4$ source. Colors show four sets of three edge points corresponding to one source disorientation with the angle $\Phi \approx 109.5^\circ$. Compare to Fig. 5 where two edge points are result of points moving on opposing faces. The third point appears as it moves from outside the fundamental cube to the third edge. Three other sets of points are similarly produced.

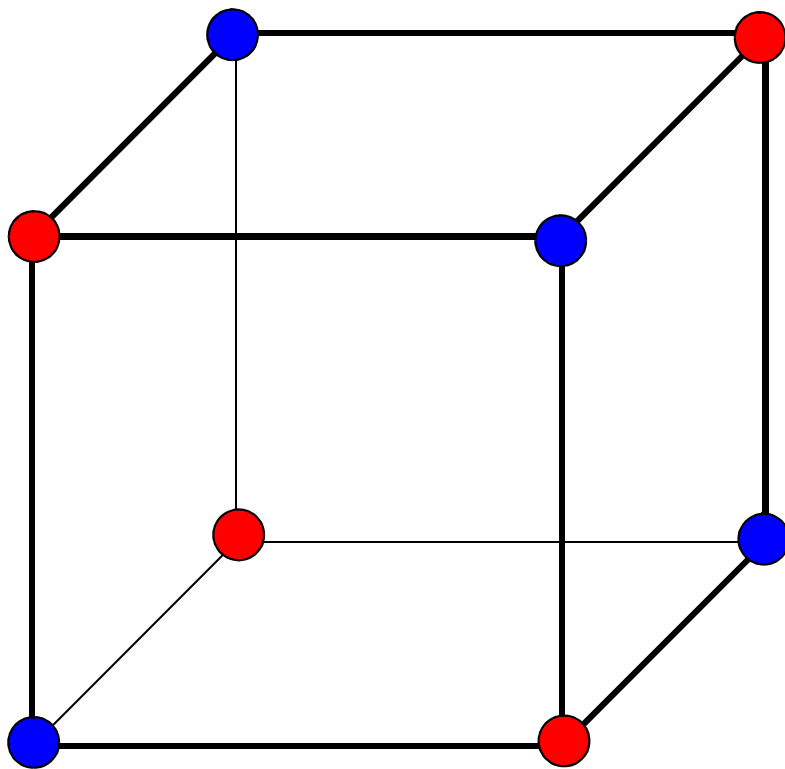


Figure 7:

Fundamental zone display for $DC4$ source. Colors show two sets of four vertex points corresponding to one source orientation with the angle $\Phi = 120^\circ$.

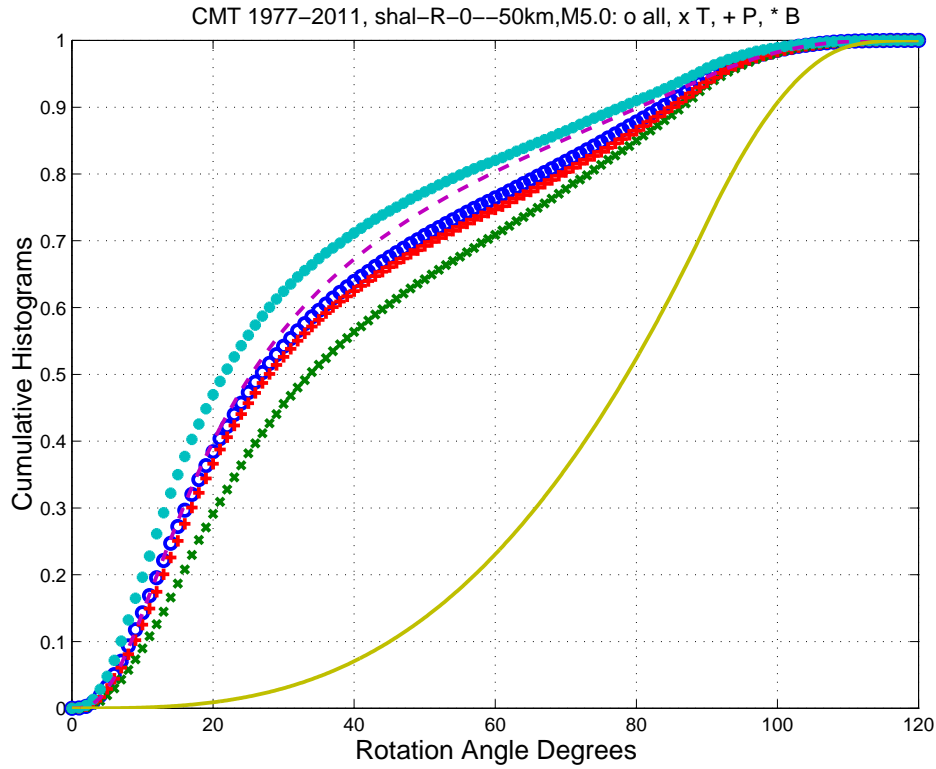


Figure 8:

Cumulative distributions of rotation angles for pairs of focal mechanisms of shallow earthquakes (depth 0-70 km) in the GCMT catalog 1977/01/01–2011/12/31; centroids are separated by distances between 0-50 km, magnitude threshold $m_t = 5.0$. The total number of events is 26,986. Lines from left to right: filled circles are centroids in 30° cones around the **b**-axis; dashed line is for the Cauchy rotation with $\kappa = 0.1$; circles – all centroids; crosses – centroids in 30° cones around the **p**-axis; x-signs – centroids in 30° cones around the **t**-axis; right solid line is for the random rotation.

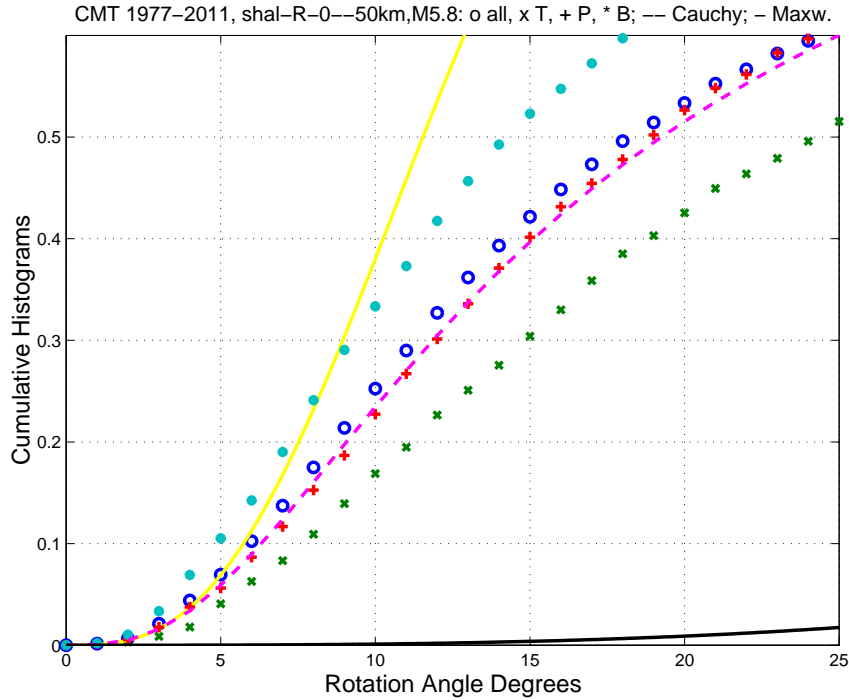


Figure 9:

Cumulative distributions of rotation angles for pairs of focal mechanisms of shallow earthquakes (depth 0-70 km) in the GCMT catalog 1977/01/01–2011/12/31; centroids are separated by distances between 0-50 km, magnitude threshold $m_t = 5.8$. The total number of events is 6,160. Lines from left to right: filled circles are centroids in 30° cones around the **b**-axis; circles – all centroids; crosses – centroids in 30° cones around the **p**-axis; x-signs – centroids in 30° cones around the **t**-axis; dashed line is for the Cauchy rotation CDF with $\kappa = 0.075$; left solid line is for the Maxwell rotation CDF (15) with $\sigma_\Phi = 7.5^\circ$; right solid line is for the random rotation.

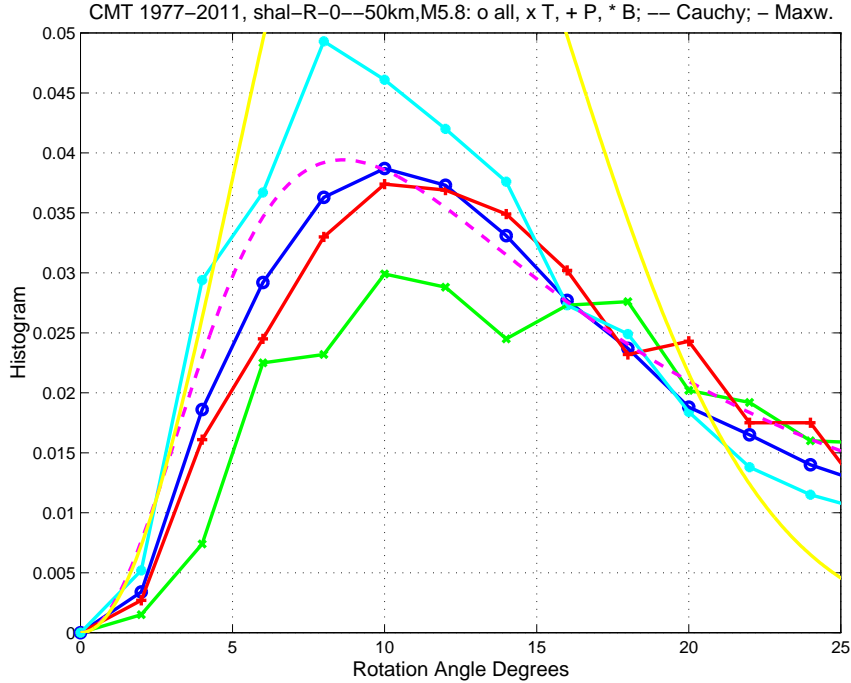


Figure 10:

Histograms of rotation angles for pairs of focal mechanisms of shallow earthquakes (depth 0-70 km) in the GCMT catalog 1977/01/01–2011/12/31; centroids are separated by distances between 0-50 km, magnitude threshold $m_t = 5.8$. The total number of events is 6,160. Lines from left to right: filled circles are centroids in 30° cones around the **b**-axis; circles – all centroids; crosses – centroids in 30° cones around the **p**-axis; x-signs – centroids in 30° cones around the **t**-axis; dashed line is for the Cauchy rotation PDF with $\kappa = 0.075$; left solid line is for the Maxwell rotation PDF (14) with $\sigma_\Phi = 7.5^\circ$.

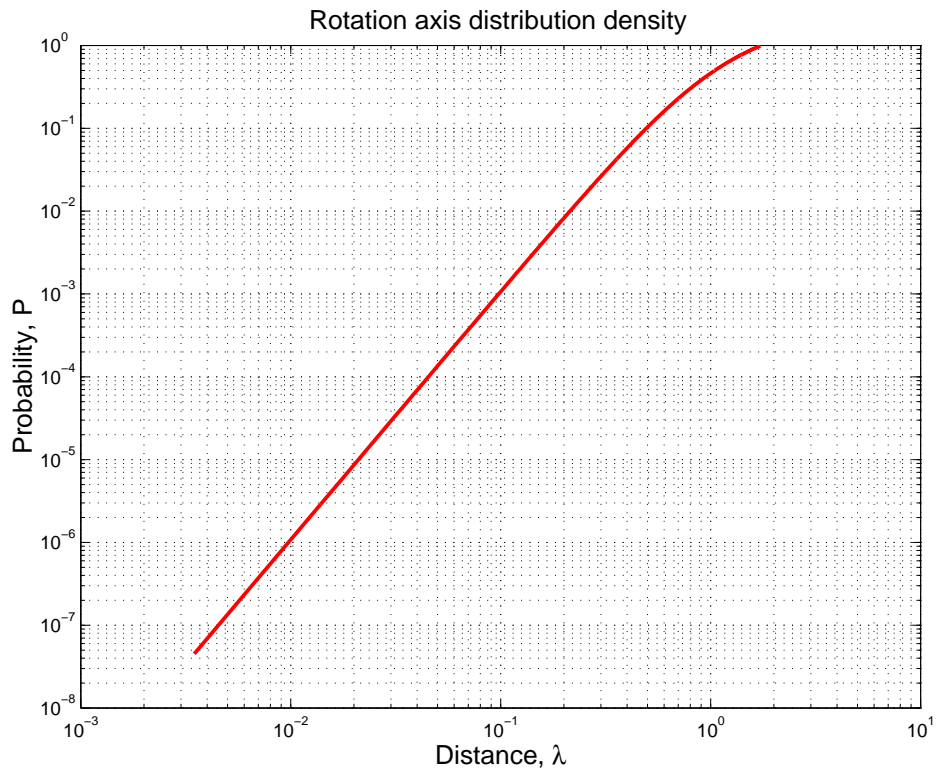


Figure 11:

Probability density function for rotation axes distribution.

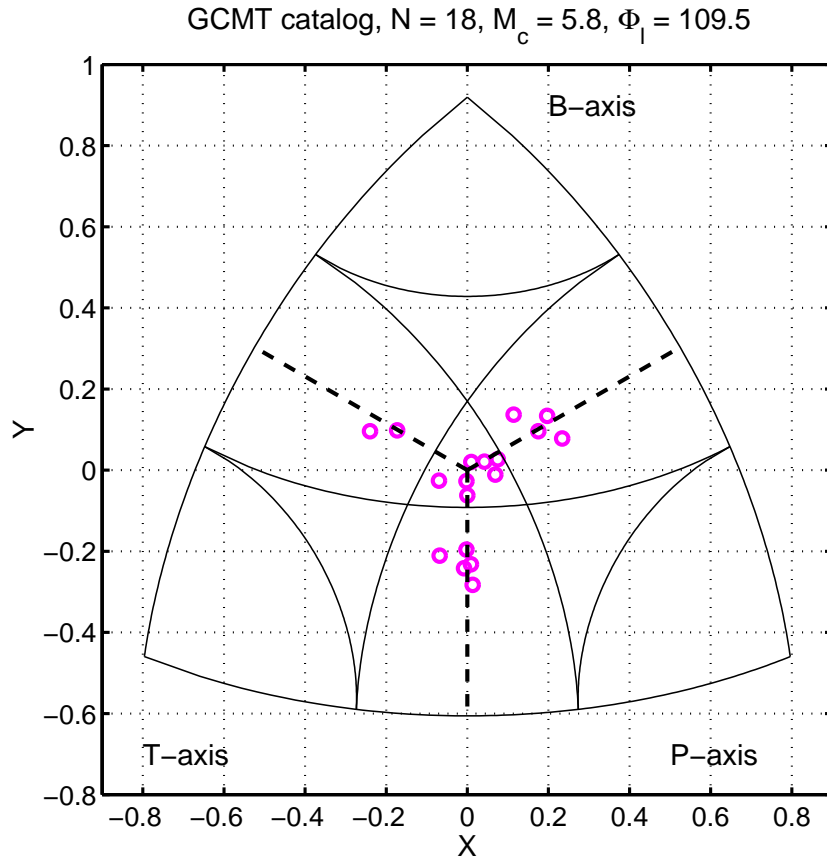


Figure 12:

Distributions of rotation poles for pairs of focal mechanisms of shallow earthquakes in the GCMT catalog. Centroids are separated by distances between 0-50 km; magnitude threshold $m_t = 5.8$; the rotation angle $109.5^\circ \leq \Phi \leq 120^\circ$.

Simulation, Iseed = 2001, N = 25000, N0 = 1754, z1 = -0.05, zu = 0.05

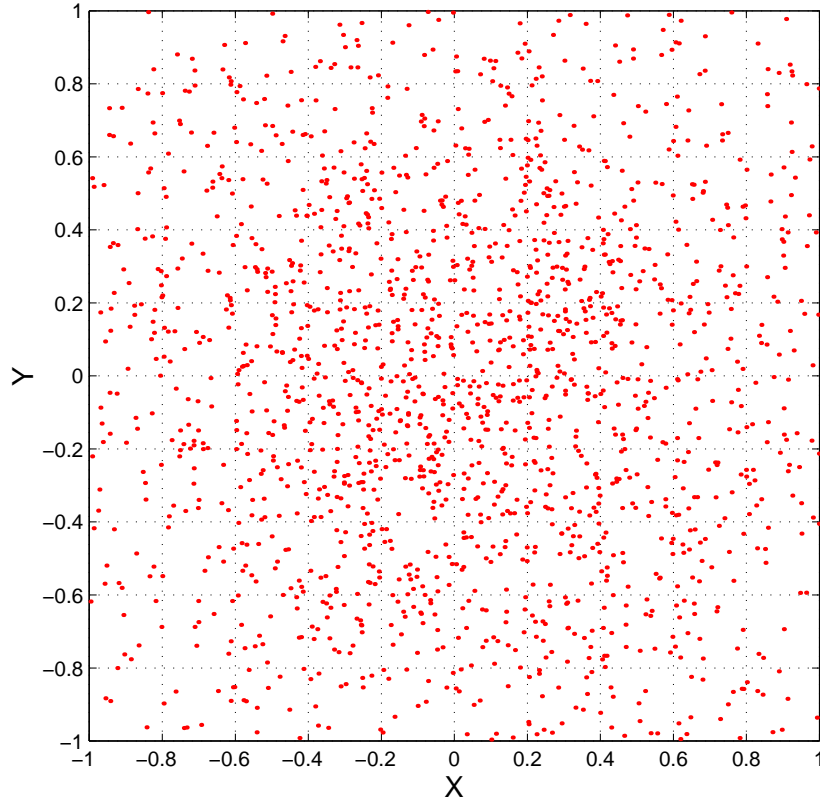


Figure 13:

Orientation distribution in the fundamental zone of the Rodrigues space for randomly rotated *DC4* sources. The points are shown in the central section of the fundamental zone $0.05 \geq x_3 \geq -0.05$ (see Fig. 4). The total point number is 25,000; 1,754 points are in the central section.

GCMT 1977–2012, $M_c = 5.8$, $N = 19397$, $N_0 = 8725$, $z_l = -0.05$, $z_u = 0.05$

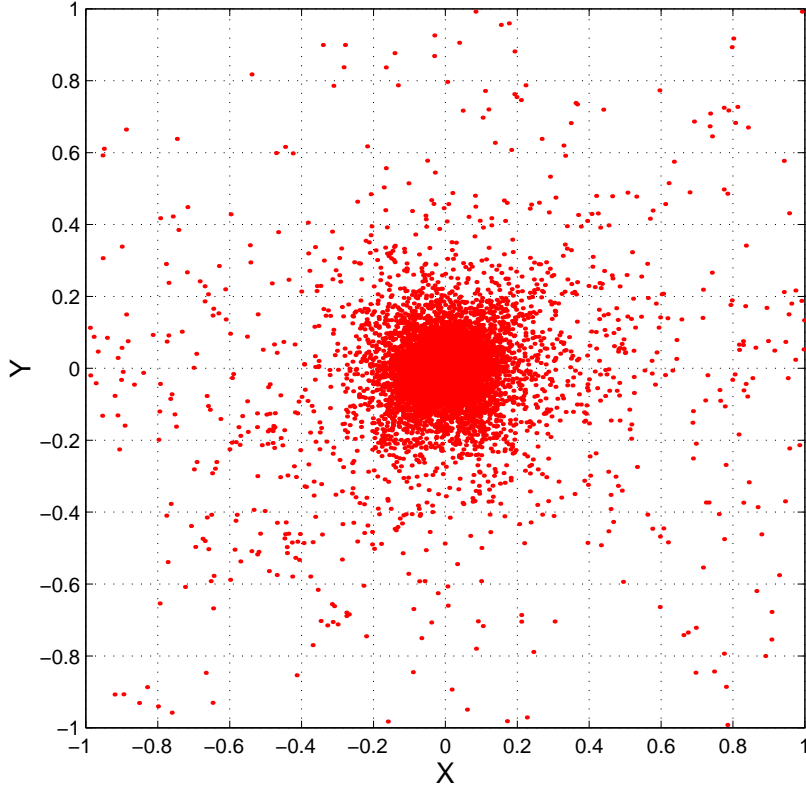


Figure 14:

Orientation distribution in the fundamental zone of the Rodrigues space for shallow earthquakes in the GCMT catalog. Centroids are separated by distances between 0-50 km; magnitude threshold $m_t = 5.8$; the total number of events is 6,160. The points are shown in the central section of the fundamental zone $0.05 \geq x_3 \geq -0.05$ (see Fig. 4). The total number of earthquake pairs is 19,397; 8,725 pair points are in the central section.